IOP Publishing Science and Technology of Advanced Materials
Sci. Technol. Adv. Mater. **10** (2009) 065002 (6pp) doi:10.1088/1468-6996/10/6/065002

Carbon nanocones: wall structure and morphology

Stine Nalum Naess[1], Arnljot Elgsaeter[1], Geir Helgesen[2,3] and Kenneth D Knudsen[1,2]

[1] Department of Physics, Norwegian University of Science and Technology, NO-7934 Trondheim, Norway
[2] Physics Department, Institute for Energy Technology, NO-2027 Kjeller, Norway
[3] Department of Physics, University of Oslo, NO-0316 Oslo, Norway

E-mail: kenneth.knudsen@ife.no

Received 22 October 2009
Accepted for publication 19 November 2009
Published 29 December 2009
Online at stacks.iop.org/STAM/10/065002

Abstract
Large-scale production of conical carbon nanostructures is possible through pyrolysis of hydrocarbons in a plasma torch process. The resulting carbon cones occur in five distinctly different forms, and disc-shaped particles are produced as well. The structure and properties of these carbon cones and discs have been relatively little explored until now. Here we characterize the structure of these particles using transmission electron microscopy, synchrotron x-ray and electron diffraction. The carbon nanocones are found to exhibit several interesting structural features; instead of having a uniform cross-section, the walls consist of a relatively thin inner graphite-like layer with a non-crystalline envelope, where the amount of the latter can be modified significantly by annealing. The cones appear with a well-defined faceting along the cone edge, demonstrating strict long-range atomic ordering; they also present occasional examples of symmetry breaking, such as two apexes appearing in the same carbon nanocone.

Keywords: nanocarbon, electron microscopy, electron diffraction

1. Introduction

Curved forms of carbon have been known to exist since the discovery of fullerenes [1] and carbon nanotubes [2, 3]. More recently, other intriguing non-planar carbon morphologies have appeared, both occurring naturally and produced synthetically [4]–[10]. Beautiful examples are the different forms of polyhedral graphite crystals as those studied by Gogotsi *et al* [6, 7]. The various ways that carbon atoms may organize with respect to each other, can conveniently be rationalized via proper combination of sp^3, sp^2 and sp^1 orbitals, as illustrated by Inagaki [11] and Dimovski [12]. Here we report a detailed structural characterization of conically shaped carbon nanoparticles resulting from a patented pyrolytic process [13]. In the work by Krishnan *et al* [14], these particles were already found to exist with five distinct apex angles, and to have an extraordinarily well-defined symmetry, determined exclusively by the topology at the cone tip. It was discovered [14] that under certain process conditions, as little as 10% of the solid output from the so-called Kvaerner Carbon Black & Hydrogen Process [13] (CBH) was in fact carbon black. The rest was a new form of carbon structures. The CBH is an emission-free industrial process that decomposes hydrocarbons directly into carbon and H_2, based on a specially designed plasma torch, with a plasma temperature above 2000 °C. The solid output consists of a significant amount of open-ended carbon nanocones (20%) [14], as well as a large number of flat carbon discs (70%), the rest being carbon black. Minute quantities of so-called fullerene cones had been discovered already in 1994 as a result of vapour condensation of carbon atoms [15], and the first theoretical studies of such structures were reported the same year [16, 17].

These carbon cones can be modelled as consisting of curved graphite sheets formed as open cones. The construction of the cones may be visualized as taking place

by cutting out sectors of $n \times 60^\circ$ ($n = 1$–5) from the flat sheet of graphene and thereafter connecting the edges. In principle, this gives dislocation-free connections. The strain at the cone apex will eventually result in n pentagons near the apex and in the nominal cone apex angles of $\alpha = 2\arcsin[(6-n)/6]$, i.e. 112.9°, 83.6°, 60.0°, 38.9°, 19.2° corresponding to 1, 2, 3, 4 and 5 pentagons, respectively [18, 19]. Note that these particles are fundamentally different from carbon nanohorns [20], naturally occurring scrolled conical carbon structures [21], as well as the multi-shell graphitic cones such as those investigated by Gogotsi *et al* [6, 7]. The latter are long needle-shaped structures where the diameter is nearly constant over the length of the particle. The nanohorns show thin fibre-like morphologies, often appearing as highly entangled chains. The scrolled conical carbon particles have a very different construction mechanism than that of the carbon nanocones described here, with the result that any apex angle, up to about 150°, can appear.

In this paper, we present some new structural information on carbon nanocones, provided by different experimental methods. Our focus is primarily on the wall structure of these nanoparticles rather than on the overall geometry which was described in [14].

2. Experimental details

Crude samples of carbon nanodiscs and nanocones, produced by pyrolysis of heavy oil using CBH, were obtained from n-TEC (Norway). Samples of this material were suspended in dimethyl sulfoxide (DMSO) (Merck, Germany) at a concentration of 10 mg ml^{-1} and sonicated for 15 min at 80 W at room temperature. Normally the samples used in electron microscopy were taken from the resulting suspensions and used without further pre-treatment.

In all cases, 20 μl of sample suspension was sprayed onto a freshly cleaved Muscovite mica (Electron Microscopy Sciences, USA) at a distance of 12 cm using the airbrush technique described by Shotton *et al* [22]. Next, the piece of mica, with Ø 30–50 μm droplets of carbon nanoparticle suspensions on top, was placed in the vacuum chamber of the freeze-fracture instrument originally described by Elgsaeter [23]. In this instrument, a Pt-film and an amorphous carbon support film, or only a carbon support film, were deposited on the samples using two separate Balzers electron beam guns. The direction in which the thin film material is deposited can be varied independently from 0° to 90° for each of the two electron beam guns. The carbon support film (10–20 nm thick) was deposited at a direction of 90° relative to the mica surface. The thin-film replica was floated off the mica surface by carefully dipping the piece of mica with the specimen replica into distilled water. The replica floating on the water surface was finally picked up on standard Ø 3 mm electron microscope grids (copper).

For the particles that were fractured with the freeze-fracture technique, about 1 μl of the DMSO-suspended samples was first placed onto 3 mm diameter copper discs. These were subsequently transferred to a precooled copper rod with a small well on top containing liquid propane. The frozen samples were finally introduced into the chamber of the freeze-fracture instrument, where cleaving was performed using a microtome arm when the chamber vacuum had reached below 1×10^{-4} Torr. During the specimen fracture process, the knife temperature was −130 to −140 °C and the specimen temperature −120 to −130 °C.

The replicas were studied using a FEI Company (USA) Tecnai 12 transmission electron microscope (TEM) set at 80 kV (100 kV for images in figures 1 and 2). The microscope is equipped with a CCD camera having a 10.8 megapixel CCD chip and 14-bit dynamic range. The electron diffraction measurements were carried out using the same instrument. The apex angles for the cones in the micrographs were measured using the angle tool in the software package ImageJ (NIH, USA).

In addition, synchrotron data for the mixed carbon particle powder were collected on the high-resolution powder diffractometer setup at beamline BM1B (SNBL) at ESRF, Grenoble. The samples for these measurements were filled in 0.3 mm boron-glass capillaries, and the x-ray wavelength was 0.375 Å.

3. Results and discussion

Based on raw material from the CBH process, we collected transmission electron micrographs of the five distinctly different types of cones present in our samples. Representative examples are shown in figures 1(a)–(d) together with an atomistic model (inset in 1(b)) of a four-pentagon cone, obtained via energy minimization of a system of atoms with the correct topology [24], as described above.

As an initial evaluation of this material, the projection apex angles θ of more than 50 cones were determined on digital electron micrographs of nanocones. When analysing these structures, one must take into account that the apex angle that appears in TEM micrographs is slightly different from the real apex angle owing to the effect of projection of the cone down to the image plane. Considering that the cross-section between cones and planes are ellipses, the following relation can be derived between the true cone apex angle, α, and the apparent apex angle, θ, of the cone projection onto the horizontal surface when the cones are lying on their side on the support film:

$$\tan(\theta/2) = \frac{1}{2}\frac{\tan\alpha}{\cos(\alpha/2)}\left[\frac{\tan\alpha}{\tan(\alpha/2)} - 1\right]^{-1/2}.$$

This formula yields the following relations between the cone angle as seen in TEM images and the actual apex angle α: $\theta = 19.4^\circ$ ($\alpha = 19.2^\circ$), 41.3° (38.9°), 70.54° (60.0°) and 126.7° (83.6°). For $\alpha = 112.9^\circ$ no cone angle appear in the projection. The subsequently obtained apex angle estimates were in good agreement with the findings reported earlier [14], with a variance of the obtained estimates less that 5% for cones with $\alpha = 19.2^\circ$, and 10% for the other values of the cone apex angles listed above. The deviations from the theoretical values are due to the thickness variation of an outer amorphous carbon layer. We return to this point later.

For a cone with apex angle α resting on a horizontal surface, it can be shown by simple geometry that a vertical cross section of the cone at a distance y from the tip

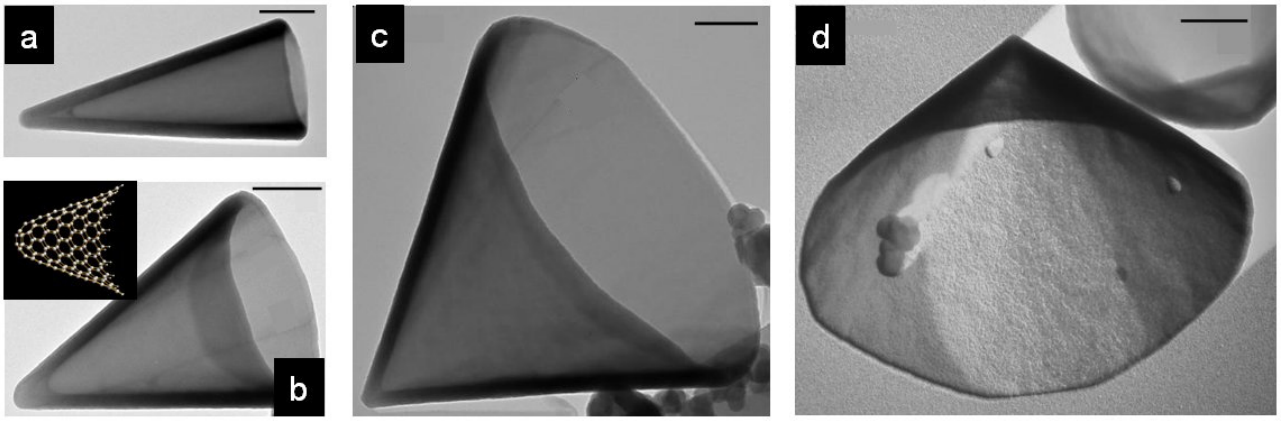

Figure 1. TEM images of carbon nanocones. (a)–(d) show cones with nominal apex angle $\alpha = 19.2^\circ$, 38.9°, 60.0° and 83.6°, respectively. The fifth cone in the series, i.e. with apex angle $\alpha = 112.9^\circ$ can be seen in figure 3(a). The inset in (b) shows an energy minimized (Car-Parinello method) atomistic model of a cone (about 200 atoms) with 38.9° apex angle, having four pentagons at the tip. (d) was shadowed at 30° with a 1–2 nm thick Pt-film in order to enhance the contrast. There is no Pt film in the specimens shown in (a)–(c). The smaller dark spherical objects in the micrographs are other forms of carbon found throughout the sample. Bar = 200 nm.

will form an ellipse with major semi-axis $b = (y/2)\tan(\alpha)$ and minor semi-axis $a = \sqrt{by\tan(\alpha/2)}$. A modelling of the electron transmission was done by stacking a number (2–5) of such conical layers with wall thickness Δt onto each other and calculating the total thickness at all points along the projection line of the vertical cut. The electron density (contrast thickness) of each layer in the model could be varied. The electron beam attenuation factor, i.e. the average Beer–Lambert–Bouguer attenuation factor K for the 100 keV beam used was $K = 0.0090\,\mathrm{nm}^{-1}$ as can be calculated from the measurements of Garberg *et al* [25] for disc-shaped particles at an electron beam energy of 80 kV using the appropriate energy and aperture corrections [26].

Figure 2(b) shows a comparison between the experimentally determined relative transmitted electron beam intensity, $I(x)/I_0$, and that calculated theoretically, along a line defined by a vertical plane located at different distances from the apex of the cone in figure 2(a). These curves show that the micrograph intensity profiles can easily be used to measure the wall thickness of these particles. The walls were best modelled using an even electron density across a wall, but there may be some small, local variations in the wall thickness and other structural inhomogeneities. The thickness varied between 10 and 30 nm, but could be as large as 80 nm for some cones.

An interesting feature of many of the carbon cones with the largest apex angles is the presence of facets at the rim of the open end of the cones. Some such facets can be discerned in figure 1(d). The micrograph may also suggest that the facets appear in pairs with one facet being larger than the other. These features are best appreciated when the cone rests on its open end as shown in figure 3(a). A few small facets can readily be seen in this figure, and inspection of the micrograph reveals an underlying five-fold rotational symmetry. This is in agreement with the predictions for such kind of structures with one pentagon at the cone tip [16, 17].

For the nanocone shown in figure 3(a) the relation between the facet interfacial angle, ϕ^{f}, and the associated projection apex angle, ϕ^{p}, reads $\tan(\phi^{\mathrm{f}}/2) = \sin(\alpha/2)\tan(\phi^{\mathrm{p}}/2)$, where α is the cone apex angle. By carefully drawing lines separating the facets in several different carbon cones, and making use of the relations described above, we find that for all cones, the facet interfacial angles of a pair of facets, ϕ_1^{f} and ϕ_2^{f}, are given as $\phi_1^{\mathrm{f}} = (22^\circ \pm 1^\circ)$ and $\phi_2^{\mathrm{f}} = 60.0^\circ - \phi_1^{\mathrm{f}}$. These values are the same as those found earlier for carbon nanodiscs [25], and correspond to Miller indices (100) and (210) of the two-dimensional hexagonal unit cell in graphite. As demonstrated by Eksioglu and Nadarajah [27], and also pointed out earlier [28], an alternating shift by $\pm 21.8^\circ$ of the crystalline axis orientation from one layer to the next in a cone or cone-helix gives an optimal graphitic alignment between the layers. Thus, it seems likely that alternating layers are here shifted by this amount, giving rise to the observed splitting of the n-fold facets into pairs of $\sim 38^\circ$ and 22° sectors. The facets seen at the open rim of the carbon cones suggest a strict long-range ordering in the cone walls at the atomic level.

Occasionally we find carbon cones which apparently have a partly completed outer layer. One such example is shown in figure 3(b). This figure indicates that cones grow in thickness by adding new layers of carbon on top of the existing nanocone walls instead of growing in length after having achieved the full wall thickness. Based on an examination of a series of analogous pictures, we believe that features such as those seen in figure 3(b) are due to the fact that two or more particles have stuck together for a certain time in the reactor chamber, thus masking some areas from obtaining the full wall thickness. These adhered particles have later been released from the cone, resulting in this particular type of imprint.

The growth processes at play in the CBH process are also capable of producing other non-regular carbon structures. Two of the most common larger structures are shown in figures 3(c) and (d). Figure 3(c) shows a nanocone with nominal cone apex angle changing from 83.6° to 38.9° at a certain distance

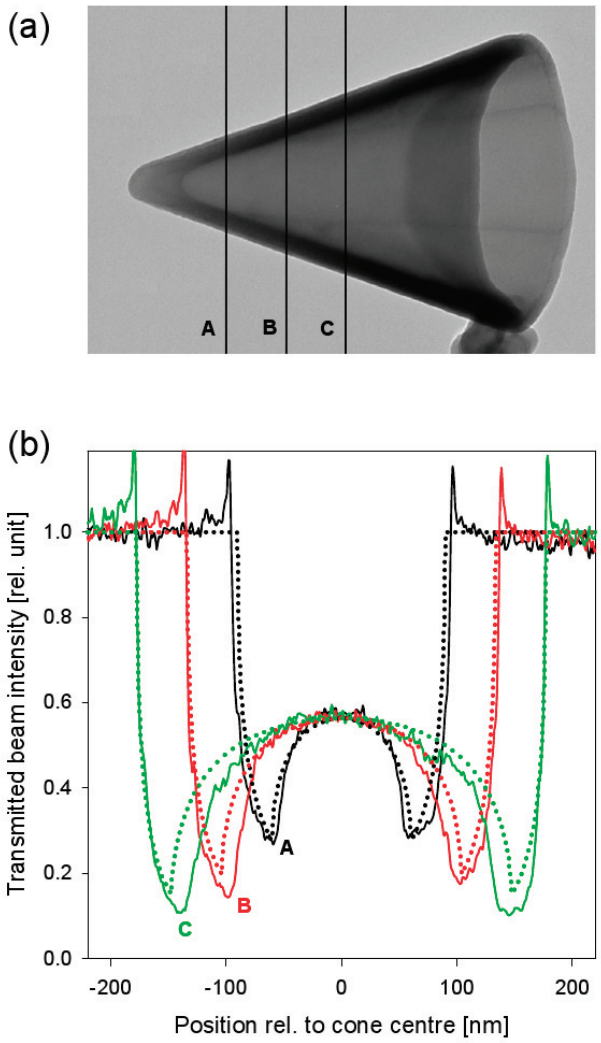

Figure 2. (a) A cone with 38.9° apex angle and (b) a comparison between the theoretically calculated electron transmission (dotted lines) and measured values (solid lines). The calculation is done along lines normal to the projection of the cone rotational symmetry axis at three different distances from the estimated cone tip, as indicated by lines in (a). The wall thickness was calculated as 28 nm.

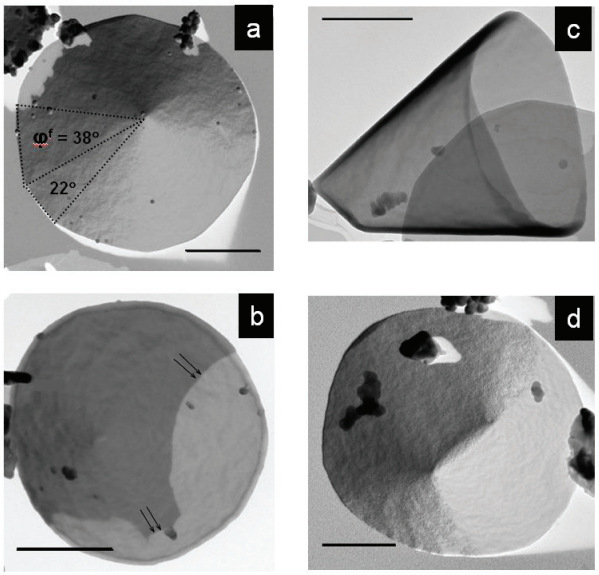

Figure 3. TEM images of different carbon cone morphologies: (a) shows a 112.9° carbon cone resting on its open end and with the apex pointing out of the image. The lines drawn out from the apex indicate the faceting of the surface, with two different facet angles. A Pt-film was here deposited at 30° relative to the horizontal plane. Bar = 1000 nm. (b) A cone with what appears to be only partly completed outer layers (edge indicated by double arrows). (c) and (d) show examples of two deformed conical carbon structures: (c) cone with nominal apex angle changing from 83.6° to 38.9° and (d) a twin-peak carbon nanocone. Bar = 500 nm. There is no Pt film in (b) and (c).

from the cone apex. This is equivalent to a transition from 2 to 4 pentagons at the tip. Because of the high electron transparency of the carbon cones, a faceted flat carbon disc present underneath this cone can readily be seen through the cone. Note also the peculiar twin peak structure in figure 3(d).

In order to elucidate better the internal composition of these particles, we induced fracture by means of a freeze fracturing setup described in details elsewhere [23]. This was most conveniently done on the carbon nanodiscs, which are the planar versions of the cones (zero pentagon analogues) that are also found in the synthesized batches. These particles were fractured after being frozen at −165 °C in a DMSO-solution, resulting in an in-plane cleavage that usually was parallel to the disc surface, as illustrated in figures 4(a) and (b).

An extensive analysis of optical density in TEM images (185 fractured particles), employing different regions of the fractured discs as indicated in figures 4(a) and (b) (inset), showed that the particles are fractured in a plane parallel to the disc surface, close to the geometrical centre of the disc, as shown by the histogram in figure 4(b). It is likely that for the discs the splitting occurs between the graphitic layers, which are only bonded by weak van der Waals forces, and not in the amorphous carbon surrounding the cone. Most of the fractures have a ratio of the thickest part x_1 to the whole disc thickness x_2 of typically $0.50 < x_1/x_2 < 0.55$. Thus, the fracture only takes place in the ∼10% central part of the disc, which then also gives an estimate of the thickness of the graphitic core, i.e. typically only 2–5 nm.

Electron diffraction was also performed on the carbon cones to determine the atomic ordering within these particles. Figure 5(b) shows a diffraction image taken near the tip of a cone, as indicated in figure 5(a). Two features are important here: (i) the symmetrical two-peak diffraction near the beam centre, indicating repeated stacking of layered carbon structures, and (ii) homogeneous rings showing the presence of amorphous carbon in the wall. The (002) reflections as indicated in figure 5(b) can be used to calculate the layer stacking in the cone wall. Using different images, we calculate the average spacing as 3.76 ± 0.10 Å, thus a layer distance which is significantly larger than in graphite. This observation is consistent with what we found earlier for carbon nanodiscs [25].

Electron diffraction in a direction perpendicular to the wall of the cone, as indicated in figure 5(c), gives a different result. Now a six-fold pattern is obtained, which is identical to that corresponding to the sp^2-hybridized in-plane ordering

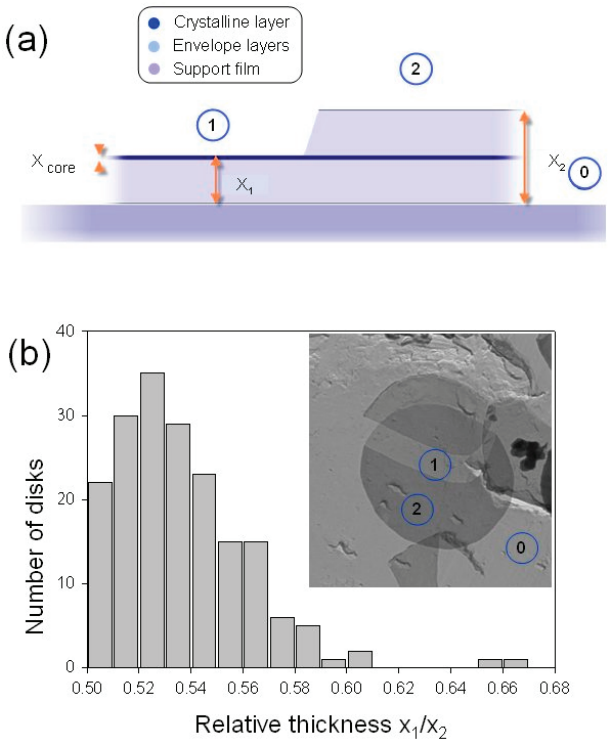

Figure 4. Fracture of carbon nanodiscs: (a) Schematic drawing of a partly fractured disc lying flat on a mica surface. x_{core}, x_1 and x_2 denote heights of the crystalline core, the lower part of the disc, and the whole disc, respectively. (b) Histogram of thickness ratio between the thickest part of the disc (after fracture) and the whole disc for a number of 185 discs with an inset showing a TEM image of a fractured disc. Regions marked 1, 2 and 0, correspond to the part of the disc left after fracture, the whole disc, and area outside the disc, respectively.

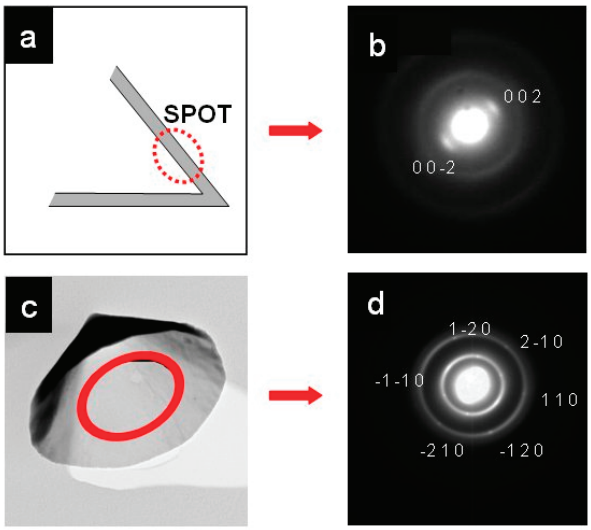

Figure 5. Setup (a) for electron diffraction (ED) along the side wall for an 83.6° cone lying on its side on the support film. The marked region indicates the area irradiated by the electron beam. (b) The corresponding ED image. (c) Setup for diffraction perpendicular to the side wall with a circle marking the region irradiated by the electron beam. (d) The corresponding ED image showing hexagonal symmetry. Some of the *hkl* reflections corresponding to the hexagonal in-plane symmetry of graphite are indicated.

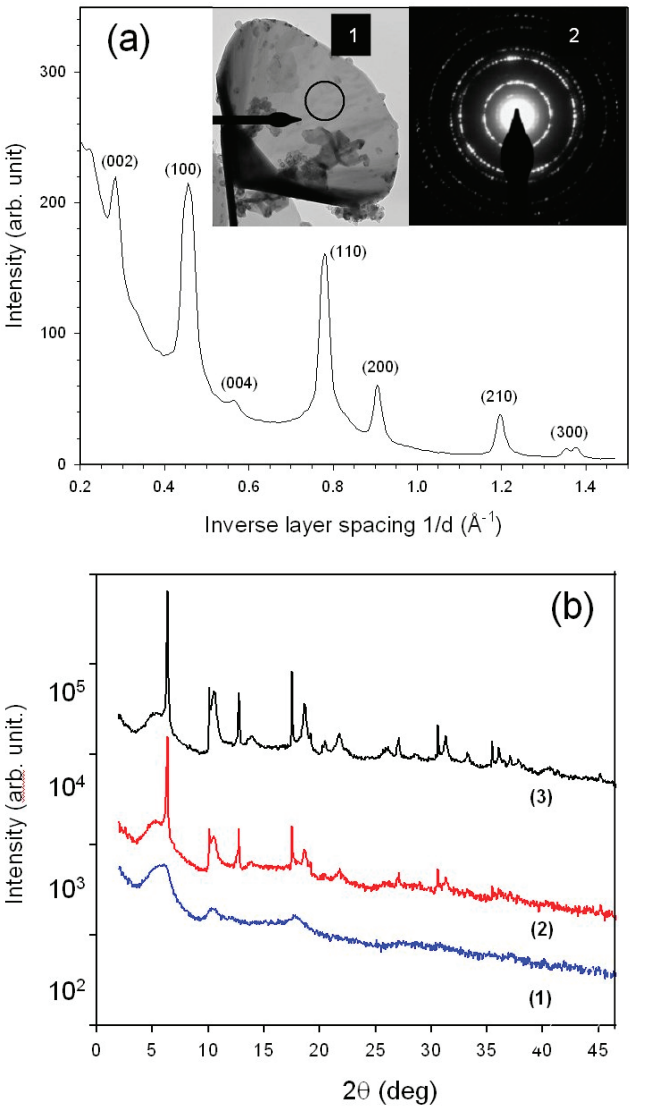

Figure 6. Properties of heat treated samples: (a) Integrated electron diffraction pattern for a heat treated cone with indexing of the *hkl* peaks. The irradiated area is marked with a circle on the cone in inset 1. The 2D diffraction pattern is shown in inset 2. (b) Synchrotron x-ray scattering data for the as-produced cone material (1) and heat-treated material (2). Graphite powder is included for comparison (3).

in graphite. Homogeneous rings of intensity are also seen in figure 5(d). Thus, it is evident from these data that the carbon nanocones consist of a graphitic core surrounded by amorphous carbon. By calculating—using the carbon discs—the relative integrated intensity of the diffraction spots compared to that of the homogeneous rings, we find that the graphitic core comprises approximately 10–30% of all the material in the particle.

If the material is heat-treated (2700 °C), the amorphous part diminishes drastically, with a corresponding increase in the amount of crystalline material. This is illustrated in figure 6(a). The synchrotron x-ray diffraction data in figure 6(b) shows that the few broad diffraction peaks of the raw material are turned into a graphitic-like pattern after heat treatment. In the electron diffraction data shown in

the inset of figure 6(a) we now find several sets of spots with six-fold symmetry, indicating an inhomogeneous nature of the graphite layer stacking. We believe this is due to crystallization taking place simultaneously in different parts of the amorphous carbon. Thus the temperature-induced conversion from amorphous carbon to layers of graphite is not fully coupled geometrically to the original graphite core, resulting in a shift in the orientation of new layers with respect to the core. For the heat-treated samples, the coherence lengths could be extracted from the diffraction pattern via measurements of the peak widths (Scherrer equation). This resulted in the coherence length of 20 nm within the graphite plane (110 reflection) and 17 nm perpendicular to the plane (002 reflection).

4. Conclusions

The presented data show that the extraordinarily symmetrical carbon nanocones produced in the Kvaerner Carbon Black & Hydrogen Process consist of a graphitic core within an envelope of non-crystalline carbon. Our data indicate that the graphitic core is first grown to its full size, whereupon layers of amorphous carbon are deposited. The core is responsible for long-range interactions at the atomic level, resulting in pairwise faceting along the edge of the cone, as seen most clearly in the five-fold symmetry for the cone with one pentagon at the tip. These cones are structurally similar to flat carbon discs reported earlier [25], and those discs can effectively be regarded as carbon cones with apex angle equal to 180°, or alternatively, with zero pentagons at the tip. The temperature history of the individual carbon cone during the pyrolytic process is probably the single most important parameter controlling the final overall structure of the particle.

The well-defined shape of these cones, their non-centrosymmetric nature, as well as recent predictions of subtle electronic properties that are distinctly different from other types of carbon—including the possibility of existing as permanent dipoles or stable conic anions and cations [24, 29]—suggest that these carbon nanoparticles can be important for understanding the structure-property relationships of carbon polymorphs in general. Applications taking advantage of this particular topology and morphology, e.g. for preferential absorption and storage of hydrogen [30, 31], can also be foreseen.

Acknowledgments

The work was in part supported by a grant to S N Naess from the Norwegian University of Science and Technology. Support from HYCONES (NMP3-CT-2006-032970) is also acknowledged. We thank the staff at the Swiss–Norwegian Beamlines at ESRF for assistance during the synchrotron measurements. Helpful discussions with and assistance from H F Cuesta, J P Pinheiro, H Heiberg-Andersen, G Kopstad, A T Skjeltorp and J Müller are gratefully acknowledged.

References

[1] Kroto H W, Heath J R, O'brien S C, Curl R F and Smalley R E 1985 *Nature* **318** 162
[2] Iijima S 1991 *Nature* **354** 56
[3] Iijima S 1991 *MRS Bull.* **19** 43
[4] Knox J H, Kaur B and Millward G R 1986 *J. Chromatography* **352** 3
[5] Endo M, Kim Y A, Hayashi T, Fukai Y, Oshida K, Terrones M, Yanagisawa T, Higaki S and Dresselhaus M S 2002 *Appl. Phys. Lett.* **80** 1267
[6] Gogotsi Y, Libera J A, Kalashnikov N and Yoshimura M 2000 *Science* **290** 317
[7] Gogotsi Y, Dimovski S and Libera J A 2002 *Carbon* **40** 2263
[8] Merkulov V I, Guillorn M A, Lowndes D H, Simpson M L and Voelkl E 2001 *Appl. Phys. Lett.* **79** 1178
[9] Terrones H *et al* 2001 *Chem. Phys. Lett.* **343** 241
[10] Ajayan P M, Nugent J M, Siegel R W, Wei B and Kohler-Redlich P 2000 *Nature* **404** 243
[11] Inagaki M 2000 *New Carbons: Control of Structure and Functions* (Oxford: Elsevier)
[12] Dimovski S 2006 Structure, characterization and exploration of synthesis of conical and polyhedral crystals of graphite *PhD Thesis* Drexel University
[13] Lynum S, Hugdahl J, Hox K, Hildrum R and Nordvik M Production of micro domain particles by use of a plasma process *Patent* EP1017622
[14] Krishnan A, Dujardin E, Treacy M M J, Hugdahl J, Lynum S and Ebbesen T W 1997 *Nature* **388** 451
[15] Ge M and Sattler K 1994 *Chem. Phys. Lett.* **220** 192
[16] Balaban A T, Klein D J and Liu X 1994 *Carbon* **32** 357
[17] Terrones H 1994 *J. Math. Chem.* **15** 143
[18] Ebbesen T W 1998 *Acc. Chem. Res.* **31** 558
[19] Heiberg-Andersen H 2006 Carbon nanocones *Handbook of Theoretical and Computational Nanotechnology* vol 8 ed M Rieth and W Schommers (Stevenson Ranch, CA: American Scientific Publishers) p 507
[20] Iijima S, Yudasaka M, Yamada R, Bandow S, Suenaga K, Kokai F and Takahashi K 1999 *Chem. Phys. Lett.* **309** 165
[21] Jaszczak J A, Robinson G W, Dimovski S and Gogotsi Y 2003 *Carbon* **41** 2085
[22] Shotton D M, Burke B E and Branton D 1979 *J. Mol. Biol.* **131** 303
[23] Elgsaeter A 1978 *J. Microsc.* **113** 83
[24] Heiberg-Andersen H and Skjeltorp A T 2005 *J. Math. Chem.* **38** 589
[25] Garberg T, Naess S N, Helgesen G, Knudsen K D, Kopstad G and Elgsaeter A 2008 *Carbon* **46** 1535
[26] Reimer L 1993 *Transmission Electron Microscopy* (Berlin: Springer)
[27] Eksioglu B and Nadarajah A 2006 *Carbon* **44** 360
[28] Amelinckx S, Luyten W, Krekels T, Van Tendeloo G and Van Landuyt J 1992 *J. Cryst. Growth* **121** 543
[29] Heiberg-Andersen H and Skjeltorp A T 2007 *J. Math. Chem.* **42** 707
[30] Skjeltorp A T and Maeland 2001 A hydrogen storage in carbon material *US Patent Specification* 6290753 B1
[31] Yu X, Tverdal M, Raaen S, Helgesen G and Knudsen K D 2008 *Appl. Surf. Sci.* **255** 1906